Fermilab Library
0 1160 0039566 9

SDC-92-199

SDC
SOLENOIDAL DETECTOR NOTES

ELECTROMAGNETIC RESOLUTION OF A TILE FIBER CALORIMETER FOR THE SDC

February 1992

Marc Turcotte
Superconducting Super Collider Laboratory

February 1992 SDC-92-199

Electromagnetic Resolution of a Tile Fiber Calorimeter for the SDC

Marc Turcotte
SSCL Physics Research Division

Abstract

The transverse electromagnetic energy resolution of a tile-fiber calorimeter has been studied using GEANT in the presence of a 2T magnetic field.

General Model Description

One of the conceptual designs of the SDC tile fiber calorimeter considered until recently has an end-cap which protudes inwards of the outer z-limit of the solenoid current sheet by an amount $\Delta_z = 15$cm. Figure 1a) is a sketch with dimensions showing the locations of various detector elements in this design. The electromagnetic setion is comprised of three separate parts: the barrel, the end-cap catcher section behind the coil and the snout section in front of the protuding or re-entrant section below the coil. All dimensions are in cm. Figure 1b) shows a detail view of the em catcher section which is concieved as an insert in the HAC1 section of the end-cap. The amount of overlap between projective lines extending from the barrel section and the em-snout section all the way to the em-catcher section is 2cm and 10cm in a variant of the geometry. [1]

The geometrical model coded into GEANT follows the dimensions showed on the figures. In particular, a 3mm gap between the edges of the plates in the em-catcher section and the hadronic section of the end-cap is used. This is consistent with possible mechanical adjustment limits. Figure 2a) shows a view of the calorimeter as rendered in GEANT. The electromagnetic compartment absorber is lead and the first hadronic section absorber is iron. No hadronic section beyond HAC1 was coded in but this has no impact for this study. In the design considered, the number of plates in the EM section is reduced from 36 at $\eta = 0$ to 21 at $\eta = 1.3$. This is to account for the $1/\sin(\theta)$ effective

1. A more recent version of the same calorimeter has a non-re-entrant flat end-cap which fixes the tracking half-length to 4m. This geometry will be considered in a separate study.

plate thickness increase and essentially to make the calorimeter a constant resolution in E_T device. Figure 2b) shows a detailed view of the barrel / end-cap region as a 20 GeV E_T shower develops in the magnetic field. The model is totally Φ-symmetric and uses a set of concentric cylinders to approximate the geometry. Table 1 lists the relevant sizes and piece counts of various elements.

The simulation uses a detailed map of the SDC solenoidal magnetic field [1]. Figure 3 shows the variation of B_z as a function of the z-distance from the Interaction Point measured in meters for various radii. For example, at the center of the SDC detector, the field strength is 2T essentially all the way to the end of the current sheet located at z = 348.6cm. The current sheet occupies the space from r=178.8cm to r=183.2cm while the solenoid cryostat extends from r = 170cm to r = 205cm.

The solenoid assembly is modeled in details following the design in Ref [2]. Figure 4 shows the thickness in radiation lengths as a function of pseudorapidity. The amount of material in the coil assembly that affects the resolution of electromagnetic showers is a function of the incidence angle and therefore, a seperate readout right behind the liner layer of the em section (massless gap readout) is included in the model. So, for barrel and end-cap, the radial segmentation is: massless gap, EM1 (first 5 layers), EM2 (all remaining layers) and HAC1. Figure 5 is a diagram of the various live and dead sections of the modeled calorimeter. Each of the 15 subdivisions records the energy deposited in the form of dE/dx both in the live (scintillator) and dead (absorber) regions. In addition, the energy deposited anywhere in the coil assembly is recorded separately. This version of the model has no pseudorapidity segmentation.

The code for the detailed description of this calorimeter was written in the SDC SHELL standards [3] and was run within that framework.

Description of the datasets

Datasets of 200 electron showers with constant initial $E_T = 20$ GeV were generated for 31 different values of η between 0.00 and 2.30 . Cascade photons were tracked down to 100 KeV and cascade electrons / positrons to 1 MeV. The simulations were run in parallel utilizing different CPU's of the SSCL PDSF computing facility either on the front end SUN's or batch ranch SGI's. Table 2 lists the total CPU time used for one of the cases considered.

At each η point, the resolution of the observed signal in the plastic was transformed to an equivalent stochastic term coefficient using the following formula:

$$E_T \text{ stochastic term coefficient} = (\sigma_E / E) \times \sqrt{20}$$

No attempt was made to simulate photostatistics fluctuations on top of the dE / dx signal. Figure 6 a) to d) show the variation of the E_T stochastic term coefficient as a function of the pseudorapidity of the incoming electrons in the case were there is no magnetic field and where there is one as descibed by the map mentioned before. For all cases, the z-point of origin of the positrons is varied about zero using a Gaussian with σ_z= 5cm. The two peaks in the curves are due to the transition regions between the barrel and end-cap catcher and between the end-cap catcher and end-cap snout respectively. The presence of the magnetic field does not affect the resolution of the electromagnetic device in the 2cm (compare 6a) and 6b)) and 10cm (compare 6c) to 6d)) overlap cases, except in the regions of complicated field configuration near the end of the current sheet and only for 10cm overlap. In the 10cm overlap case and only for the cross-over region around η = 1.55 there is a slight improvement of the resolution from turning the field on (compare 6c) to 6d)). However, there is a worsening of the resolution this time between the 2cm overlap and 10cm overlap cases in both field-off (compare 6a) to 6c)) and field-on (compare 6b) to 6d)) and again only for the larger eta cross-over. Surprisingly, the larger overlap case (10cm) has a slightly worse resolution at the larger eta transition, field-on or field-off, although in the field-on configuration, the difference is very slight. In the lower eta transition, data from the 2cm and 10cm overlap cases (field-on and field-off) are compatible. Note that no correction for the presence of the dead material was attempted in any of these runs.

The peaks in the cross-over regions are due to showers being initiated / measured partly in the barrel and partly in the end-cap catcher or snout region. Following the approach in Ref. 4, the total energy deposited in the plastic readout of the electromagnetic compartment is written as

$$E_{sum} = E_{plastic} + \alpha_{mg} E_{mg}$$

where E_{mg} and $E_{plastic}$ refer to the integrated dE / dx over a cascade in the massless gap layer and the sum of all the other layers respectively. The massless gap weight factor α_{mg} is extracted using the following expression:

$$\alpha_{mg} = [(E_{incident} - E_{leakeage}) \times SF - E_{plastic}] / E_{mg}$$

for each value of η where SF is the sampling fraction of the calorimeter as determined

by the simulation. The values obtained for α_{mg} vary from 2.57 at $\eta = 0$ to 3.24 at $\eta = 1.45$. Figure 7a) to 7d) show the result of the scans in the 2cm and 10cm overla- geometries, field-off and field-on and with a massless gap correction applied whe possible. Starting at $\eta = 1.5$ there is no longer enough (or any) material in front of the electromagnetic compartment (since the simulation does not include any detector component inwards of the solenoid coil) so that the massless gap correction cannot be calculated. In these cases, the weight is set to unity. The massless gap correction factors are determined only for fully contained showers well away from the cross-over points (barrel to em-catcher and em-catcher to em-snout). For the cases where the showers develop directly in the cross-over regions, the massless gap factors computed for the nearest fully contained showers on either sides are used. Also, when combining the energy detected in the plastic readout in the barrel with that in the end-cap, it is necessary to correct for the difference in sampling fractions. The massless gap technique is clearly very effective in recovering much of the resolution loss in the lower η transition where it can be used. For example, compare 6b) to 7b) or 6d) to 7d) for the field-on 2cm and 10cm overlap cases. After massless gap correction, an overlap of 10cm is also slightly preferred (compare 7b) to 7d) in the lower η region).

Conclusions

The presence of the magnetic field has little effect on the resolution except in the high eta cross-over region where it seems to bring a slight improvement. A larger amount of overlap is favored in the lower eta cross-over region (10cm over 2cm and using the massless gap correction). Above all, the massless gap technique shows to be useful in recovering much of the electromagnetic resolution loss in the complicated cross-over region. Indeed, in the 10cm overlap case after massless-gap correction, the acceptance under the first peek (above the average response in the barrel away from the end) is 2% of the pseudorapidity range 0 to 3. If the good electron acceptance criterion is set at 25% for the stochastic term coefficient, there is then no loss of acceptance in the first transition. However, this current round of simulations did not include the effect of tracking devices (and associated cabling) and of the solenoid coil supports which all add to the amount of dead material upstream of the calorimeter.

Acknowledgements

Many thanks to Craig Blocker, Chris Hearty and Jim Siegrist for countless useful discussions, to Jimmy Proudfoot for suggesting investigating the cross-over regions as a function of the overlap, and to Bob Kephart and Bob Wands for the use of maps of the SDC magnetic field in the presence of the iron in the hadronic sections of the calorimeter. Also, thanks to Dave Coupal for the use of his single particle gun generator.

Figure Captions

Figure 1a) Sketch of the GEANT geometry. All dimensions are in centimeters. The model consists of a realistic coil, EM and HAC1 compartments in a barrel and end-cap.
Figure 1b) Details of the electromagnetic end-cap catcher section behind the coil. The overlap in the cross-over sections is 2cm.

Figure 2a) Geometry as depicted by GEANT graphics. The view is in the rz-plane with z increasing towards the right of the diagram.
Figure 2b) A 20 GeV E_T shower developing in the em-snout at $\eta = 1.55$. The dotted (full) lines are cascade photons (electrons/positrons). Notice the charged backwards flow transported in the magnetic field just below the coil and the curling charged particle tracks in the region above and beyond the end of the current sheet.

Figure 3 B_z component of the solenoidal magnetic field at various radii. At the center of the detector, the magnetic field strength is approximately constant and equal to 2T dropping rapidly beyond the end of the current sheet. Notice the field direction reversal just beyond the outer radius of the solenoid assembly (at r = 2.05m) and further into the barrel electromagnetic compartment (at r = 2.188m).

Figure 4 Thickness of the coil assembly (measured in units of radiation lengths) as a function of the pseudorapidity of the incoming positrons.

Figure 5 Sketch of the locations and numbering of the various energy sums kept in the simulation. Each number refers to either the absorber or the read-out sum. The energy deposited in the coil assembly is also recorded. The model does not have segmentation in pseudorapidity.

Figure 6a) E_T resolution stochastic term coefficient as a function of pseudorapidity with the magnetic field turned off and 6b) turned on. For these two cases, the amount of overlap in the cross-over regions was 2cm. Figure 6c) and 6d) are the equivalent figures for 10cm overlap. In all cases, the origin of the incident positrons was varied about the center of the detector using a Gaussian with $\sigma_z = 5$cm and the transverse energy was 20 GeV. The peaks in the response curves are associated with the cross-over regions between the barrel and end-cap catcher and the end-cap catcher and end-cap snout.

Figure 7a) to d) E_T resolution stochastic term coefficient as a function of pseudorapidity with the magnetic field turned on, the I.P. z-position jittered ($\sigma_z = 5$cm) and for fixed 20 GeV transverse energy in two overlap geometries (2cm and 10cm). The circles indicate points where a massles gap correction was done to restore linearity and improve the resolution. Squares indicate points for which no massless gap correction could be derived and unity weight was used.

Table 1

List of components with sizes and counts.

Component	Barrel EM		End-Cap EM catcher		End-Cap EM snout	
Skin (s. steel)	.3175	(×1)	.3175	(×1)	.3175	(×1)
MG plastic	.4	(×1)	.4	(×1)	.4	(×1)
Absorber (Pb)	.3175	(×36, ×21)	.635	(×22)	.635	(×22)
R/O plastic	.4	(×36, ×21)	.4	(×22)	.4	(×22)

[All dimensions are in centimeters]

Table 2

Total CPU time required to run the GEANT simulation on the Silicon Graphics computers of the PDSF batch ranch facility in seconds. The rur included the IP position jitter and full tracking in the magnetic field.

η	E [GeV]	Run time [sec]
0	20.0000	22 415
.25	20.6283	23 383
.5	22.5525	23 357
1	30.8616	34 233
1.25	37.7685	41 386
1.26	38.0908	49 133
1.27	38.4168	48 313
1.28	38.7468	53 652
1.29	39.0806	60 049
1.3	39.4183	65 533
1.31	39.7599	66 644
1.32	40.1056	59 745
1.33	40.4552	53 307
1.34	40.8089	56 408
1.35	41.1667	46 037
1.4	43.0180	47 636
1.45	44.9768	53 290
1.5	47.0482	54 309
1.51	47.4764	n / a
1.52	47.9094	n / a
1.53	48.3471	n / a
1.54	48.7897	n / a
1.55	49.2372	89 941
1.56	49.6896	n / a
1.57	50.1469	n / a
1.58	50.6093	n / a
1.59	51.0767	61 256
1.6	51.5493	57 412
1.8	62.1495	58 950
2.05	78.9664	75 433
2.3	100.744	91 144

References

[1] Bob Wands, FNAL.

[2] Solenoidal Detector Workshop, KEK, Japan, 1990, p145.

[3] SDC SHELL Documentation, D. Adams and S. Kunori; coordinators.

[4] C. Hearty, SDC Note # 90-00145 (November 1990).

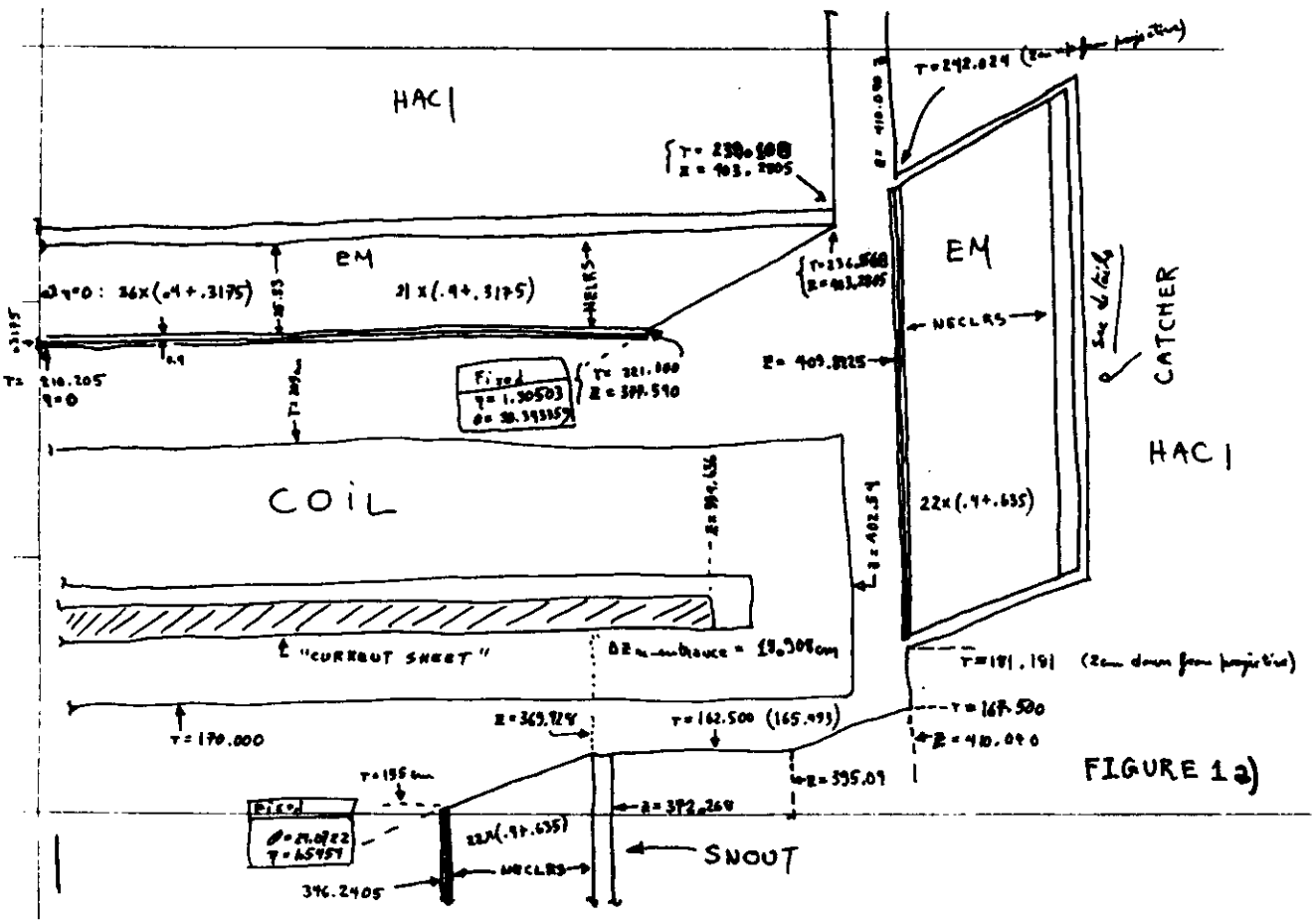

FIGURE 1a)

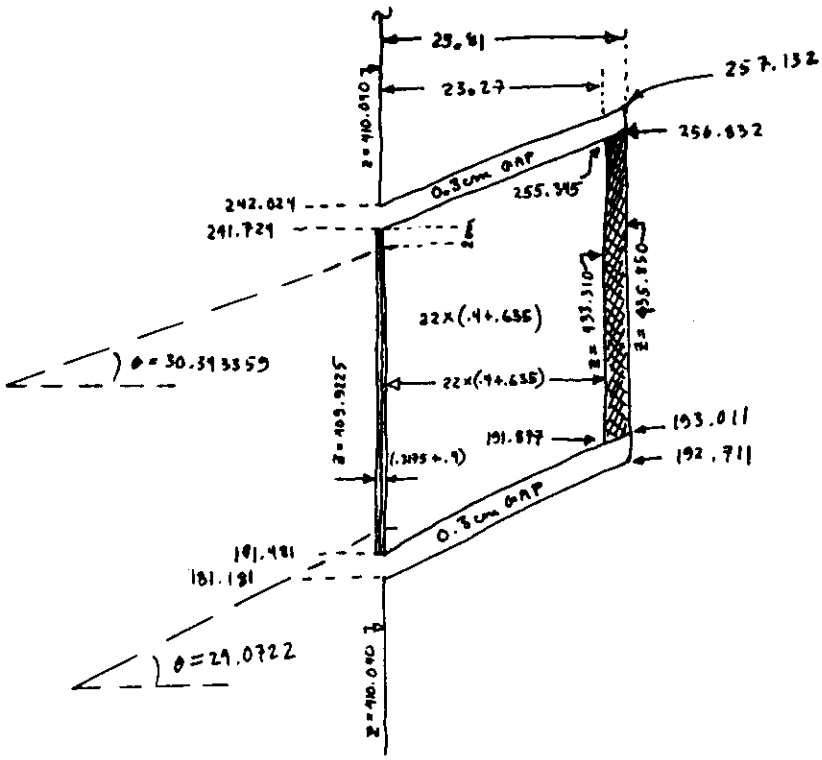

CATCHER DETAILS

2cm overlap.

FIGURE 1b)

FIGURE 2a)

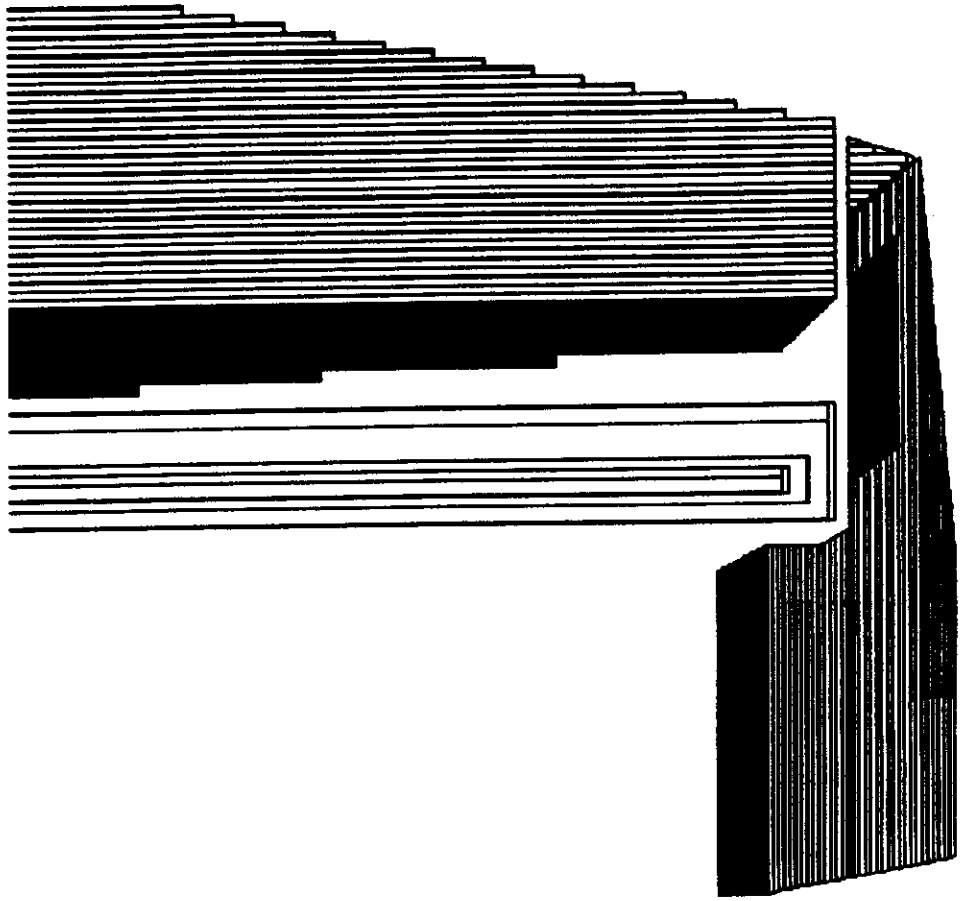

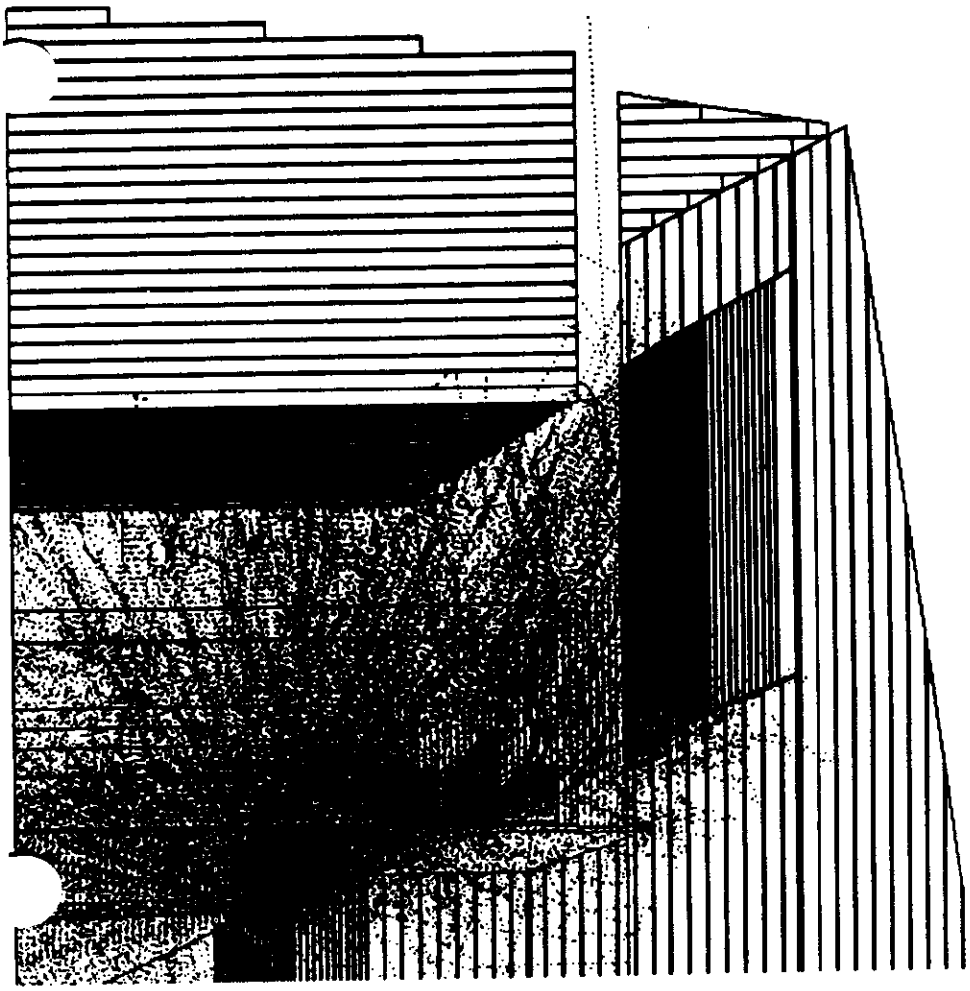

FIGURE 2b)

coil_3846_map.dat

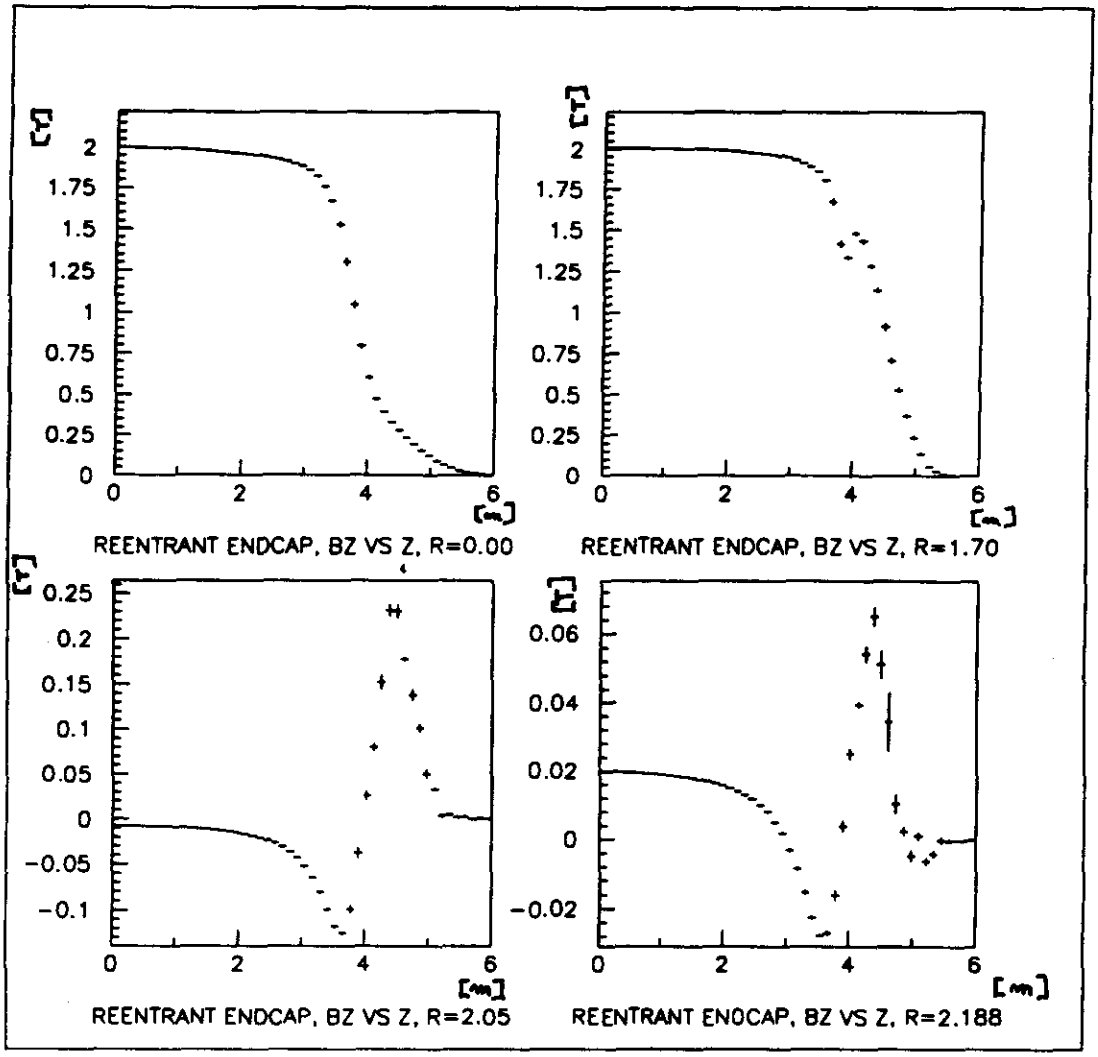

FIGURE 3

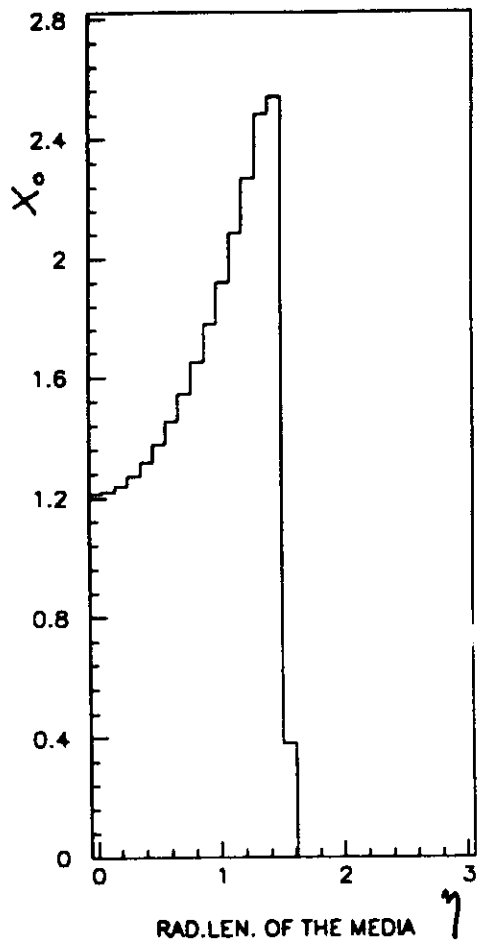

FIGURE 4

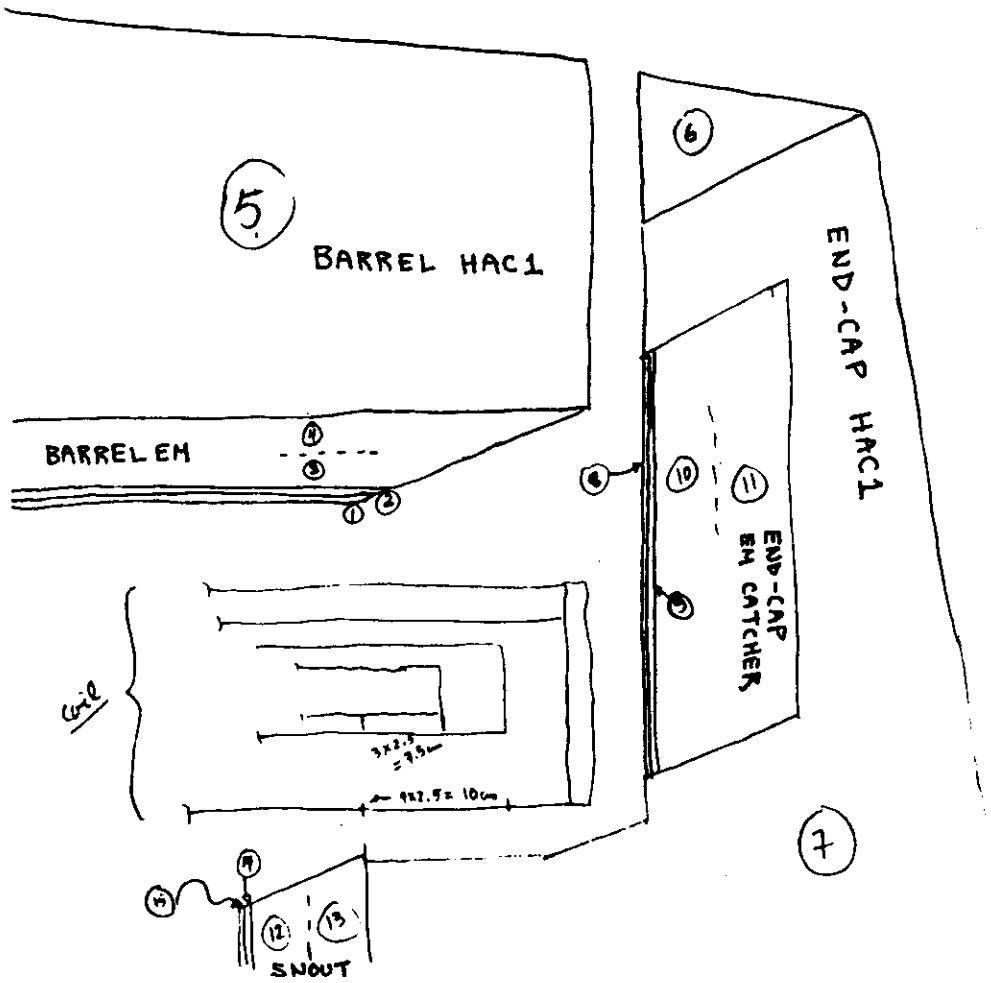
END-CAP HAC1
6
7
END-CAP EM CATCHER
11
10
9
8
BARREL HAC1
5
BARREL EM
4
3
2
1
Coil
3x2.5 = 7.5cm
22.5x 10cm
14
15
16
12
13
SNOUT

FIGURE 5

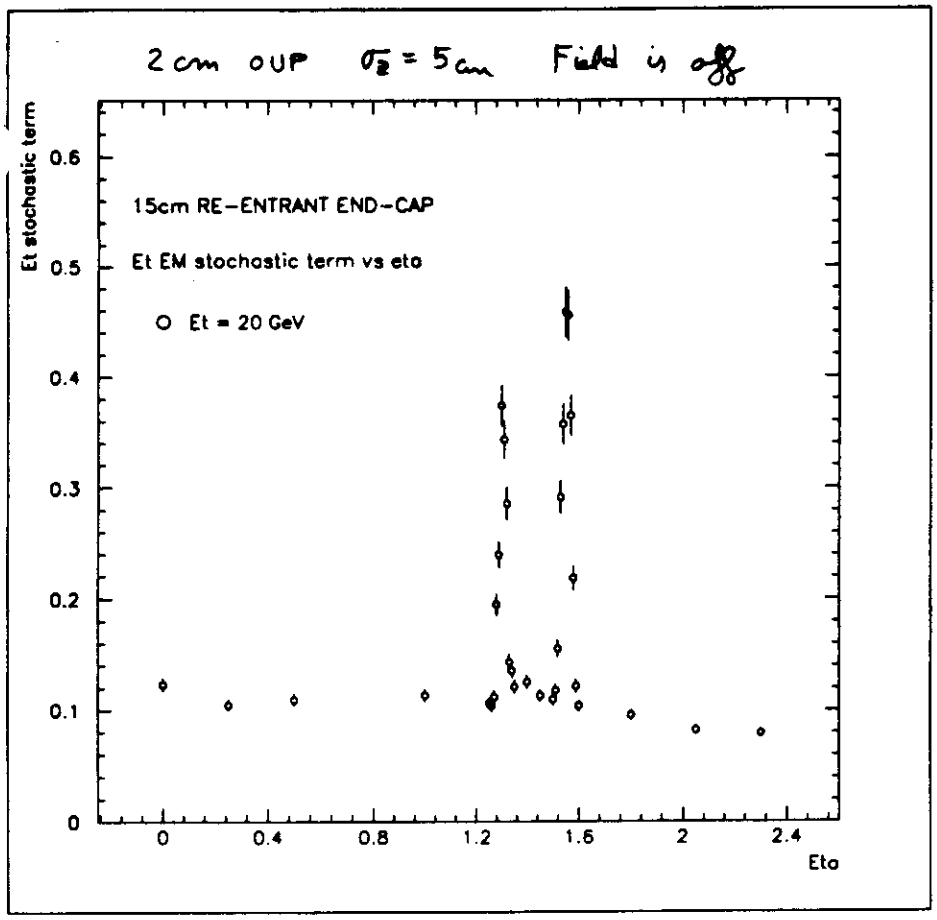

Figure 6a)

Figure 6b)

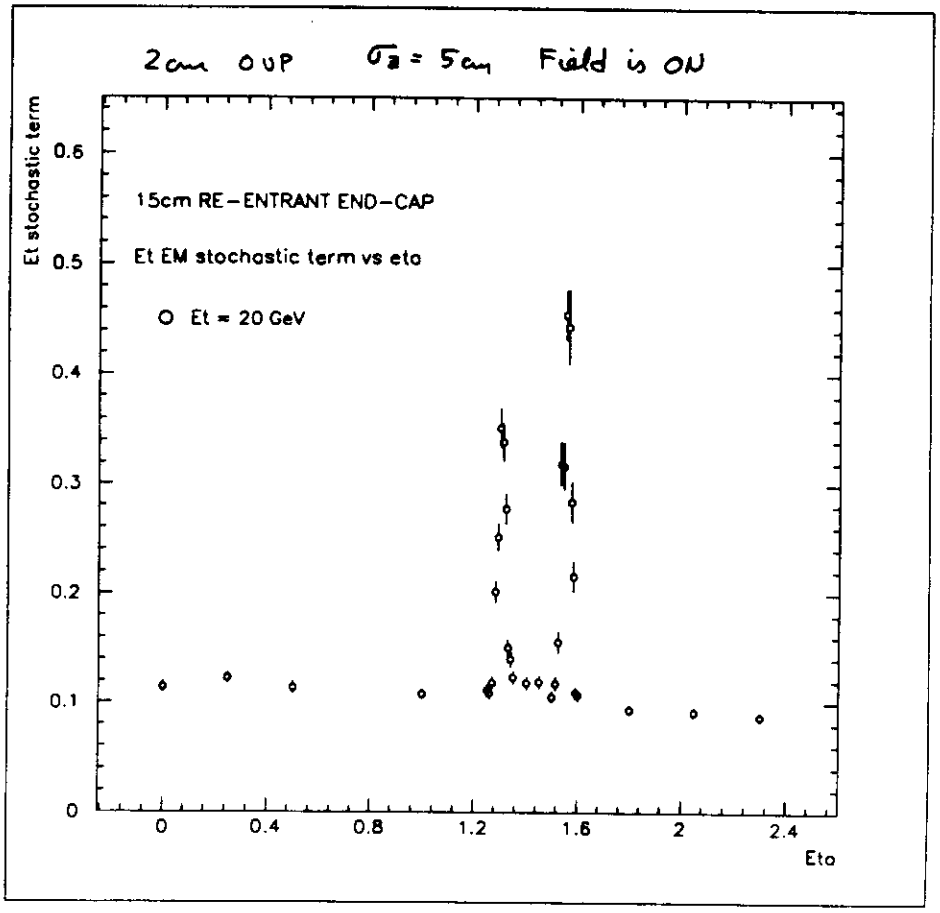

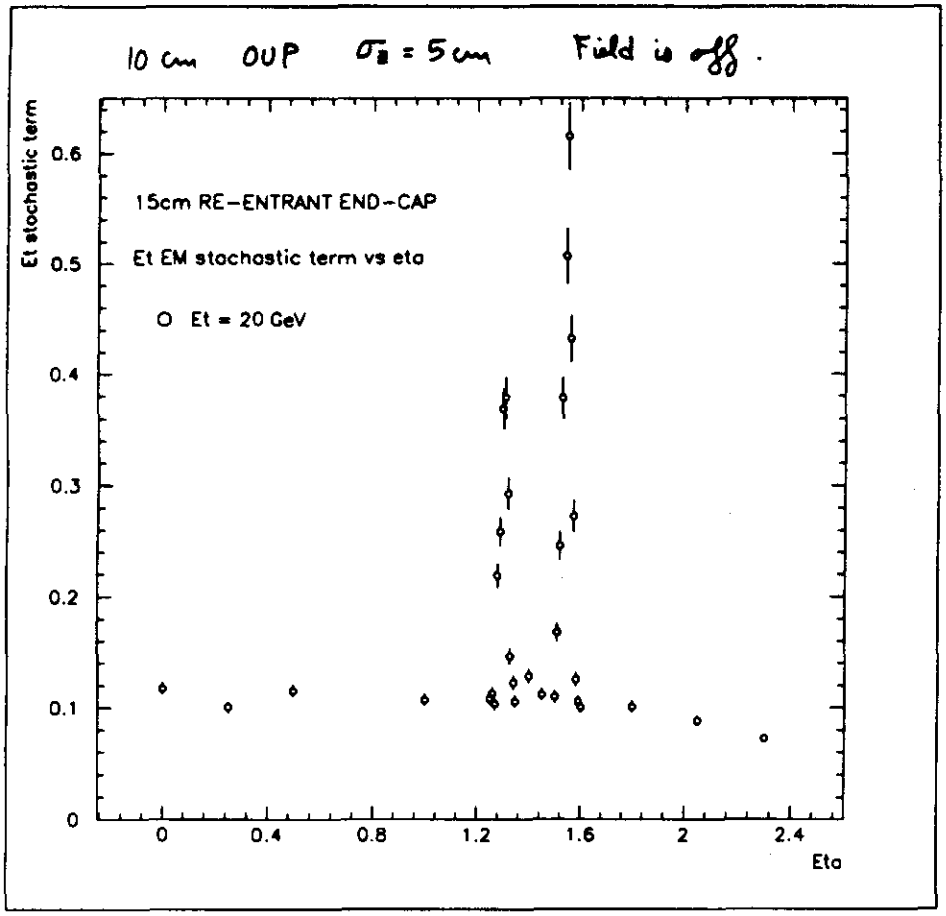

Figure 6c)

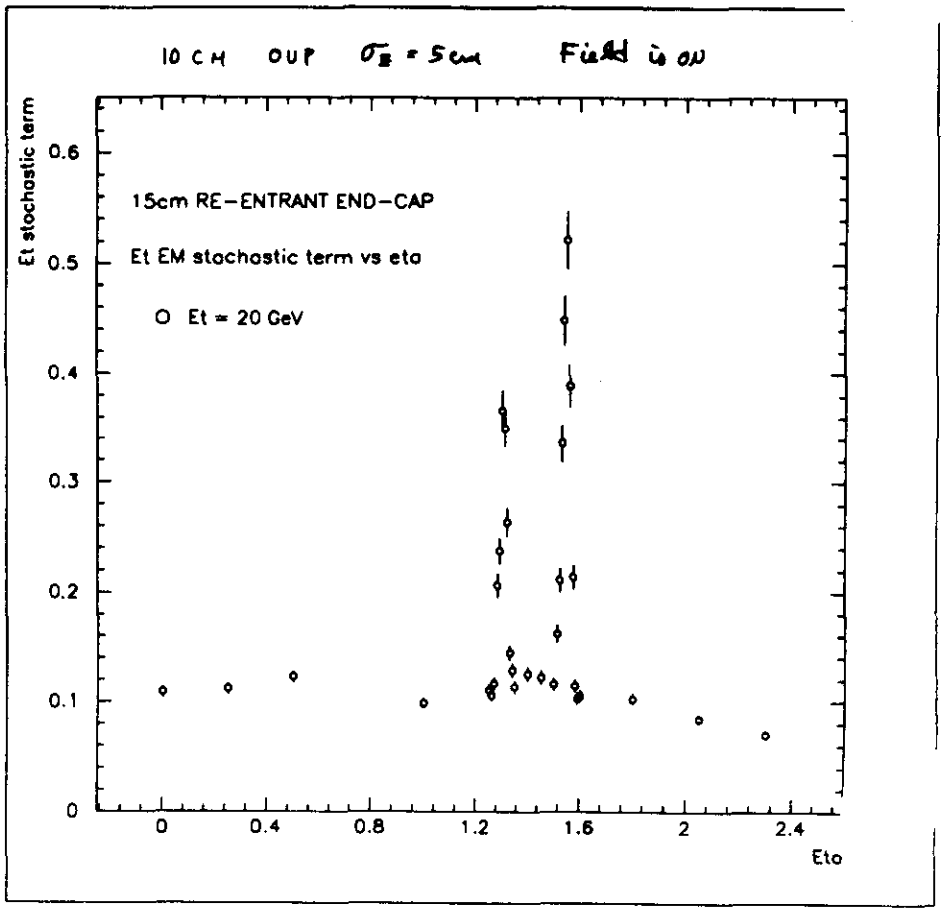

Figure 6d)

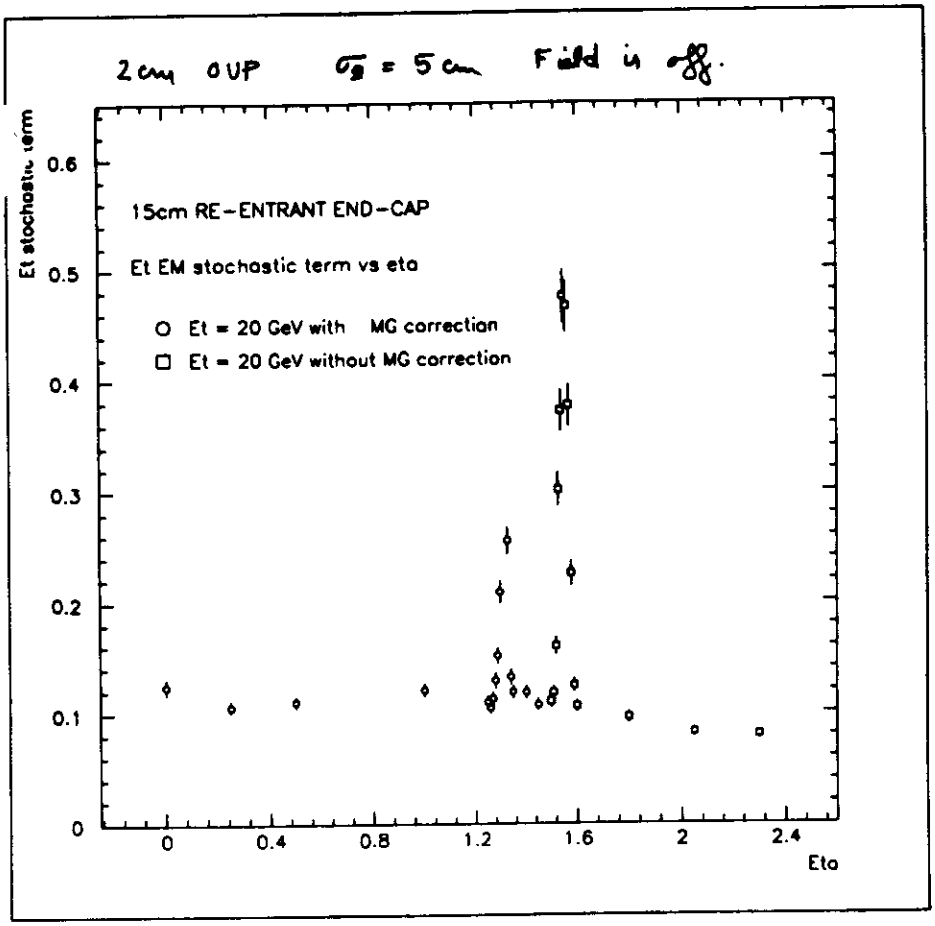

Figure 7a)

FIGURE 7b)

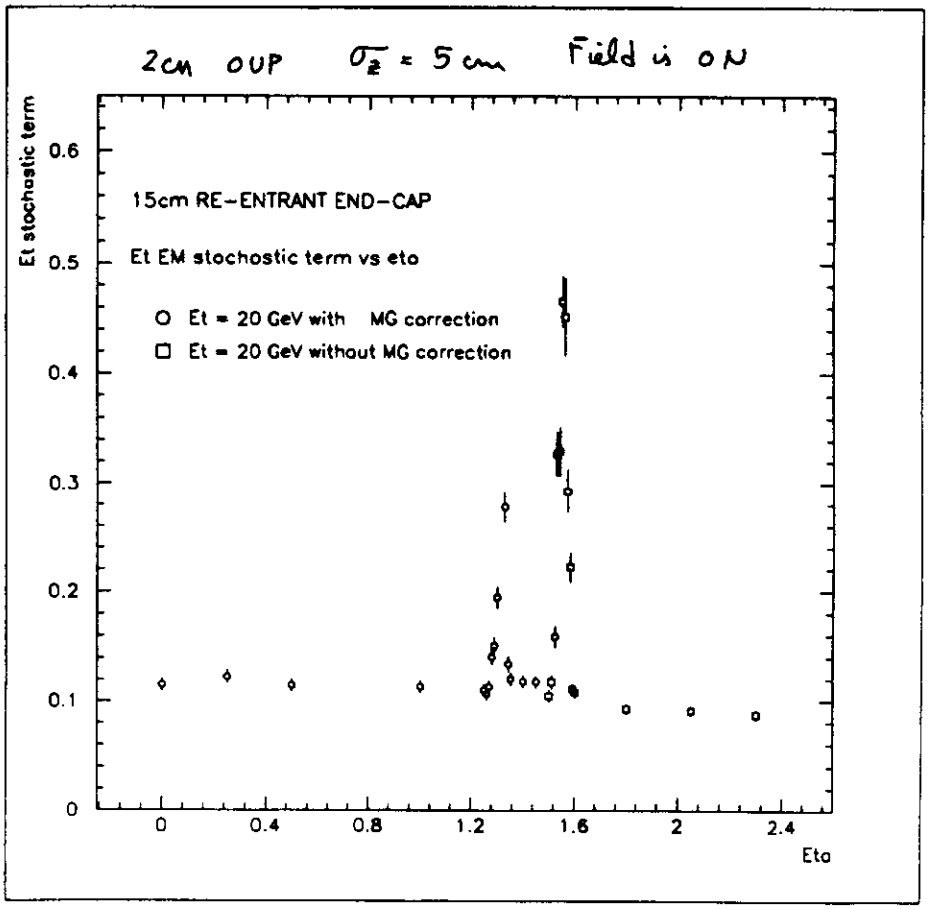

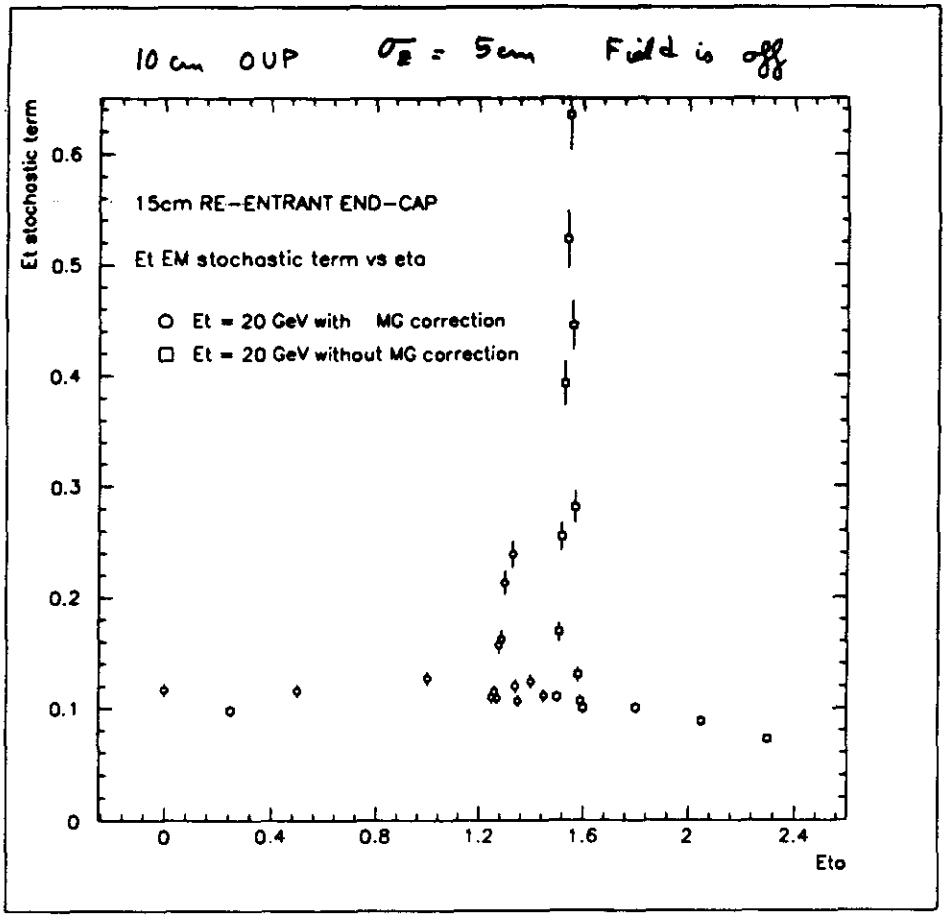

Figure 7c)
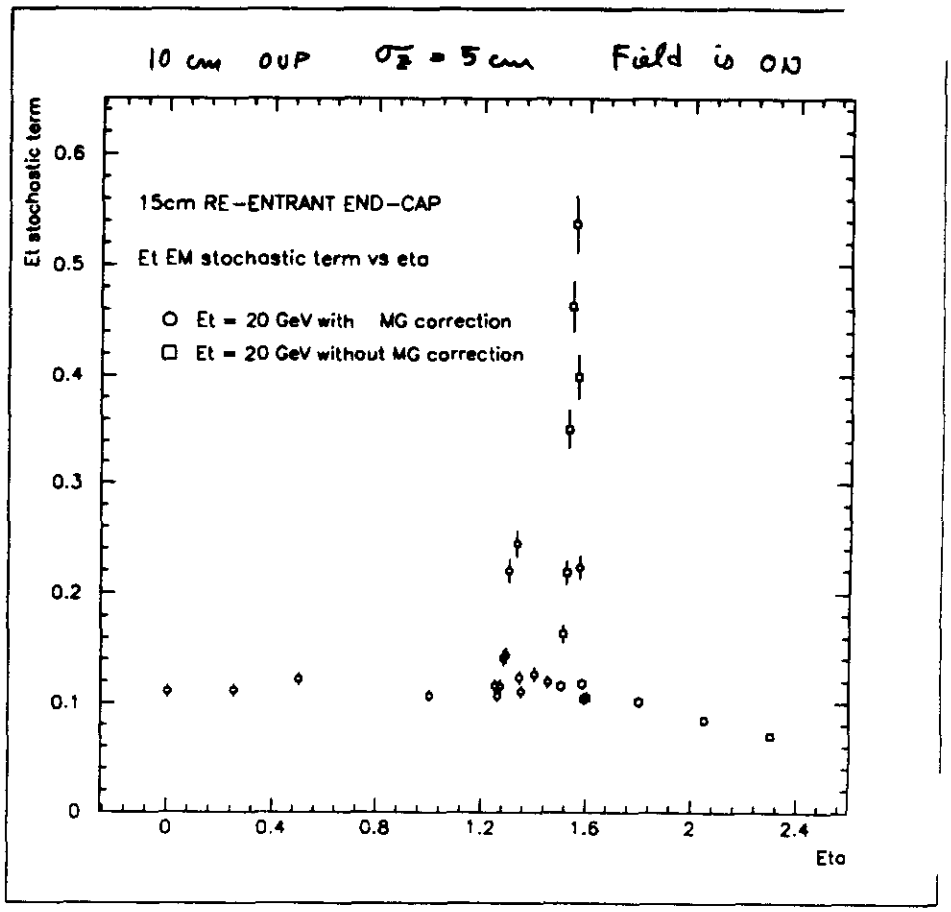
FIGURE 7d)